

Frustrated quantum critical theory of putative spin-liquid phenomenology in 6H-B-Ba₃NiSb₂O₉

G. Chen, M. Hermele, and L. Radzihovsky

Department of Physics, University of Colorado, Boulder, CO 80309, USA

(Dated: June 18, 2022)

A recently discovered material, 6H-B-Ba₃NiSb₂O₉ was found to display unusual low-temperature phenomenology, interpreted as a quantum spin liquid with spin $S = 1$ on a triangular lattice. We study a spin $S = 1$ quantum exchange model on an AB stacked triangular lattice near its quantum paramagnet-to-spiral magnet transition, driven by easy-plane single-ion anisotropy. We demonstrate that the frustrated inter- and intra-layer exchange interactions induce contour lines of low energy excitations that lead to a broad crossover regime of linear-temperature dependence of the specific heat. Based on this and a variety of other predictions, we argue that the observed phenomenology can be understood in terms of a conventional picture of a proximity to this frustrated critical point.

PACS numbers: 71.70.Ej, 71.70.Gm, 75.10.-b

Recent years have seen intense experimental and theoretical activity in the search for quantum spin liquids (QSLs). QSLs are Mott insulators that remain magnetically disordered down to zero temperature, and, as we use the term here, are also exotic states of matter, characterized by properties such as quantum number fractionalization, topological order, and gapless excitations in the absence of spontaneously broken symmetry. The realization of QSLs in theoretical models has been well established[1], and a number of materials have emerged as promising candidates[2–9]. However, there is still no direct confirmation of QSL physics in any of these systems. Thus, it is important to consider alternative explanations for the apparent QSL behavior that has been observed. Indeed, such explanations now exist for some former and current QSL candidates[10–14].

Most of the current QSL candidates share a basic rough phenomenology: they are electrical insulators, but with thermodynamic properties similar to those of a metal. In particular, many of these systems have a Pauli-like (*i.e.* constant) low-temperature magnetic susceptibility, and a linear temperature dependence of the low-temperature specific heat. Theoretical attempts to explain this behavior usually invoke $S = 1/2$ fermionic spinons with a constant density of states, and it has been challenging to find alternative explanations.

Recently the compound 6H-B-Ba₃NiSb₂O₉ (6H-B) has been proposed as a QSL candidate[15]. This system has magnetic ions Ni²⁺ forming triangular layers with local spin moment $S = 1$. The Curie-Weiss temperature is $\Theta_{\text{CW}} = -75.5\text{K}$ and no sign of magnetic ordering is detected down to 0.35K, which indicates a strong frustration. The system exhibits the QSL phenomenology described above, with a linear temperature dependence of specific heat and constant spin susceptibility at low temperatures[15]. To account for these experiments, both Refs. 16 and 17 proposed QSLs with fermionic spinons. In contrast to these two interesting exotic proposals, in this Letter we argue that the 6H-B data can be understood without invoking QSL physics. We propose that the putative QSL behavior arises as a crossover tied to the proximity of a quantum critical point (QCP) between a magnetically-ordered spin spiral state favored by the frustrated exchange interactions, and

a quantum paramagnetic (QP) phase, favored by single-ion anisotropy. It should be emphasized that our theory relies crucially on the characteristic features of the 6H-B system, and does not generalize to other QSL candidates.

In 6H-B, the Ni²⁺ triangular layers have an A-B stacking with the lattice sites on one layer projecting to the centers of the triangle plaquettes on the two neighboring layers (see Fig. 1). Our minimal model includes the interlayer (J_1) and intralayer (J_2) spin exchange and a single-ion spin anisotropy. Treating the two neighboring triangular layers as the two sublattices of a honeycomb lattice, we view the system as a multilayer honeycomb lattice. Therefore, when the exchange is dominant and frustrated, the classical ground state is highly degenerate[18]. Quantum fluctuation lifts the degeneracy and favors coplanar spiral orders. A strong on-site easy-plane anisotropy favors a quantum paramagnetic ground state, which is separated from the ordered state by a QCP. We propose that 6H-B is close to this QCP, and may lie either on the QP or magnetically ordered side. The constant spin susceptibility arises from the explicit breaking of spin rotational symmetry by the single-ion anisotropy, and the powder nature of these samples. More notably, we interpret the observed broad linear-temperature specific heat as an intermediate regime that arises from an approximate constant density of states (DOS) at intermediate energies.

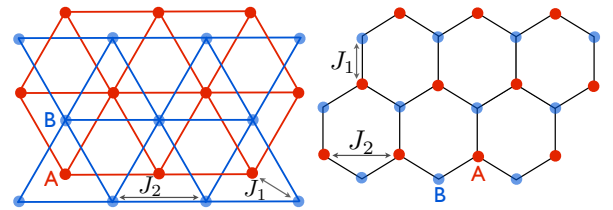


FIG. 1. (Color online) The bilayer triangular lattice (left) is equivalent to a single layer honeycomb lattice (right). J_1 , J_2 are interlayer and intralayer exchange, respectively.

Hamiltonian for 6H-B—We consider both the interlayer and intralayer exchange interaction for 6H-B. Although the interlayer exchange path goes through one more oxygen than

the intralayer coupling, the multiplicity of the former path is larger than the latter. In addition, in a structurally similar material 6H-A-Ba₃NiSb₂O₉ with long-range magnetic order, the specific heat at low temperature is observed to behave as $C_v(T) \sim T^3$, which indicates a non-negligible interlayer coupling. The interlayer coupling may thus play an important role in understanding the properties of the 6H-B material. The resulting exchange model is thus given on the triangular multilayers with the following Hamiltonian,

$$\mathcal{H}_{\text{ex}} = J_1 \sum_{\langle ij \rangle \in \text{AB}} \mathbf{S}_i \cdot \mathbf{S}_j + J_2 \sum_{\langle ij \rangle \in \text{AA and BB}} \mathbf{S}_i \cdot \mathbf{S}_j, \quad (1)$$

in which, the first sum is for the interlayer exchange between nearest neighbor (NN) sites on neighboring A and B layers, the second sum is for the intralayer exchange between NN sites within the same layer. As illustrated in Fig. 1, the interlayer (intralayer) exchange on a triangular bilayer can be viewed as the nearest neighbor (next nearest neighbor) exchange on a single honeycomb layer. In contrast to Ref. 16, we do not include the NN biquadratic exchange (that can arise from high order perturbation of the Hubbard model or effectively from spin-lattice interaction), that we expect to be strongly subdominant to the exchange \mathcal{H}_{ex} .

In addition to the exchange, we also include the single-ion anisotropy. The magnetic ion Ni²⁺ carries a spin $S = 1$ which admits a single-ion anisotropy in a non-cubic environment. The space group symmetry P6₃mc of 6H-B restricts the single-ion anisotropy to have the following form,

$$\mathcal{H}_{\text{ani}} = D \sum_i (S_i^z)^2, \quad (2)$$

where the z axis is normal to the triangular layers. Since an easy-axis anisotropy is more likely to favor magnetic order, we expect an easy-plane anisotropy with $D > 0$ for 6H-B, where such order is not observed.

Minimal model for 6H-B—Our model thus contains two competing terms, exchange and single-ion anisotropy,

$$\mathcal{H} = \mathcal{H}_{\text{ex}} + \mathcal{H}_{\text{ani}}. \quad (3)$$

For this minimal Hamiltonian, we implement high temperature series expansion and extract the Curie-Weiss temperature. We thereby find that $\Theta_{\text{CW}}^z = -[4(J_1 + J_2) + D/3]$ and $\Theta_{\text{CW}}^\perp = -[4(J_1 + J_2) - D/6]$ for magnetic field applied along and perpendicular to the z axis, respectively. With a powder sample in experiment[15], after a powder average we have $\Theta_{\text{CW}}^{\text{av}} = -4(J_1 + J_2) = -4J$ which is independent of the anisotropy parameter D , and where $J \equiv J_1 + J_2$. Furthermore, as the spin susceptibility starts to saturate at around 25K[15], using the Weiss mean-field theory described below, we establish that this saturation temperature is set by D . We thus expect D to be comparable to J .

For the minimal Hamiltonian in Eq. (3), when the single-ion anisotropy \mathcal{H}_{ani} dominates with $D \gg J$, the ground state is a uniform QP state with $|S^z = 0\rangle$ at each site. In the opposite

limit of dominant exchange, we expect the ground state to be magnetically ordered. Luttinger-Tisza method[19] gives the classical ground state spin configurations with the ordering wavevector $q_z = 0$ and spins lying in the xy plane. With $q_z = 0$, the exchange is equivalent to a $J_{\text{eff}}\text{-}J_2$ model on a 2D honeycomb lattice with $J_{\text{eff}} = 2J_1$ [18]. When $J_1 > 3J_2$, the classical ground state is a usual Néel state. When $J_1 < 3J_2$, the classical ground state is degenerate with degenerate spin spiral wavevectors $\mathbf{q}_\perp = (q_x, q_y)$ satisfying,

$$\sum_{\{\mathbf{b}\}} \cos(\mathbf{q}_\perp \cdot \mathbf{b}) = \left(\frac{J_1}{J_2}\right)^2 - 3, \quad (4)$$

in which, $\{\mathbf{b}\}$ are 6 next-nearest neighbor (NNN) lattice vectors of the honeycomb lattice. The degenerate wavevectors form contour curves in momentum space. Moreover, in the limit of $J_1 \ll J_2$, this spin spiral reduces to a commensurate spiral state corresponding to the familiar 120° of the decoupled A and B triangular lattices. Quantum fluctuations lift the degeneracy of these classical spin-spiral ground states, selecting states characterized by a discrete set of \mathbf{q} 's around which the quantum zero-point energy is minimized. Remarkably, the classical ground states favored by the quantum fluctuation do not vary upon introducing the single-ion anisotropy. The optimal spin spiral wavevectors are given by[18]

$$\mathbf{q}_\perp = \left(0, \frac{2}{\sqrt{3}} \cos^{-1} \left(\left(\frac{J_1}{2J_2}\right)^2 - \frac{5}{4} \right) \right), \quad \text{for } 1 < \frac{J_1}{J_2} < 3 \quad (5)$$

$$\mathbf{q}_\perp = \left(2 \cos^{-1} \left(\frac{J_1}{2J_2} + \frac{1}{2} \right), \frac{2\pi}{\sqrt{3}} \right), \quad \text{for } \frac{J_1}{J_2} < 1, \quad (6)$$

the other five equivalent wavevectors are obtained by $\pi/3$ rotations about Brillouin zone (BZ) center from the above result. Generally, these states are incommensurate spirals.

Weiss mean-field theory—Starting from the magnetically ordered phase, the existence and properties of the phase transition can be analyzed within a standard mean-field theory (MFT). We decouple the exchange interaction into an effective Zeeman field which is then self-consistently determined for each sublattice. We parameterize the spin order as,

$$\begin{aligned} \mathbf{S}_A(\mathbf{r}) &= M[\cos(\mathbf{q} \cdot \mathbf{r})\hat{x} + \sin(\mathbf{q} \cdot \mathbf{r})\hat{y}], \\ \mathbf{S}_B(\mathbf{r}) &= M[\cos(\mathbf{q} \cdot \mathbf{r} + \phi)\hat{x} + \sin(\mathbf{q} \cdot \mathbf{r} + \phi)\hat{y}]. \end{aligned} \quad (7)$$

in which, ϕ is the relative phase between two sublattices that depends on J_1/J_2 , and M is magnetic order parameter to be determined self-consistently. This parameterization describes both the Néel state for $J_1 > 3J_2$ and the incommensurate spin spiral states for $J_1 < 3J_2$, with the 120° state as the limiting case $J_1 \ll 3J_2$ of the triangular lattices. Zero-temperature MFT yields that in the vicinity of the QCP the magnetic order parameter is

$$M = \sqrt{2(1 - D/D_c)} \quad (8)$$

with the critical anisotropy parameter $D_c = 12(J_1 - J_2)$ for the Néel state when $J_1 > 3J_2$, $D_c = 6J_2$ for the 120° state at

vanishing J_1 , and $D_c = 6J_2 + 2J_1^2/J_2$ for the incommensurate spin spiral state when $J_1 < 3J_2$. We expect that as usual the mean-field analysis overestimates D_c (see Fig. 2).

Within this MFT, we also study the magnetization process for the QP phase in external magnetic fields. For field applied along z axis, the zero-temperature susceptibility vanishes. For field applied along x (or y) axis, the zero-temperature spin susceptibility saturates to a constant

$$\chi_0^\perp = \frac{2\mu_0(g\mu_B)^2}{D + 12J}. \quad (9)$$

In a powder sample (studied in experiments), the zero-temperature spin susceptibility averages to $\chi_0^{\text{av}} = 2\chi_0^\perp/3$.

Mean-field theory from paramagnetic phase—It is convenient to model this easy-plane system with rotor variables, by introducing an integer-valued field n_i and 2π -periodic phase variable ϕ_i , which satisfy $[\phi_i, n_j] = i\delta_{ij}$. With the mapping, $S_i^z \rightarrow n_i$ and $S_i^\pm \rightarrow \sqrt{2}e^{i\phi_i}$, the rotor Hamiltonian reads

$$\mathcal{H}_{\text{rotor}} = \frac{1}{2} \sum_{ij} J_{ij} [2 \cos(\phi_i - \phi_j) + n_i n_j] + \sum_i D n_i^2, \quad (10)$$

where J_{ij} takes J_1 (J_2) for NN interlayer (intralayer) bonds. Although n_i only takes the values of $\pm 1, 0$ in the spin model, due to the substantial anisotropy D , we expect that relaxing this restriction is unlikely to have significant effects.

Using a standard coherent state path integral, we integrate out the field n_i and obtain the partition function,

$$\mathcal{Z} = \int \mathcal{D}\Phi \mathcal{D}\lambda e^{-S - i \sum_i \int d\tau \lambda_i (|\Phi_i|^2 - 1)}. \quad (11)$$

Here,

$$S = \int d\tau \sum_{\mathbf{k}} (4D\mathbb{I} + 2\mathcal{J}_{\mathbf{k}})^{-1}_{\mu\nu} \partial_\tau \Phi_{\mu,\mathbf{k}}^* \partial_\tau \Phi_{\nu,-\mathbf{k}} + \sum_{ij} J_{ij} \Phi_i^* \Phi_j, \quad (12)$$

we have represented $e^{i\phi_i}$ by the unimodular field Φ_i^* , $\mathcal{J}_{\mathbf{k}}$ is the 2×2 exchange coupling matrix written in momentum space, μ, ν are the sublattice indices, and \mathbb{I} is a 2×2 identity matrix. The unimodular constraint on Φ_i is enforced by the Lagrange multiplier fields λ_i . We proceed by introducing a saddle-point approximation; by assuming $i\lambda_i = \beta\Delta(T)$ at the saddle point, we integrate out the Φ field and obtain the saddle-point equation (SPE) for $\Delta(T)$ in QP phase,

$$\sum_{i=\pm} \int_{\mathbf{k} \in \text{BZ}} \frac{d^3\mathbf{k}}{u_{\text{BZ}}} \frac{2D + s_{i,\mathbf{k}}}{\epsilon_{i,\mathbf{k}}} \coth\left(\frac{\beta\epsilon_{i,\mathbf{k}}}{2}\right) = 2, \quad (13)$$

where $u_{\text{BZ}} = 16\pi^3/\sqrt{3}$ is the volume of 3D BZ, $s_{\pm,\mathbf{k}} \equiv \pm 2|J_1 \cos(\frac{k_z}{2})| \sqrt{3 + \sum_{\{\mathbf{b}\}} \cos(\mathbf{k} \cdot \mathbf{b})} + J_2 \sum_{\{\mathbf{b}\}} \cos(\mathbf{k} \cdot \mathbf{b})$ are the eigenvalues of $\mathcal{J}_{\mathbf{k}}$, and $\epsilon_{\pm,\mathbf{k}}$ are the two spin excitation modes,

$$\begin{aligned} \epsilon_{\pm,\mathbf{k}} &= \sqrt{(4D + 2s_{\pm,\mathbf{k}})(\Delta(T) + s_{\pm,\mathbf{k}})} \\ &= \sqrt{2[(s_{\pm,\mathbf{k}} + D + \frac{\Delta(T)}{2})^2 - (D - \frac{\Delta(T)}{2})^2]} \quad (14) \end{aligned}$$

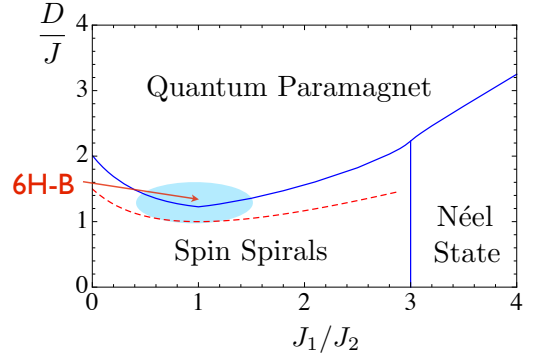


FIG. 2. (Color online) Zero-temperature phase diagram determined from the SPE in Eq. (13). Shaded region (in blue) is the expected parameter regime for the 6H-B compound. Dashed (red) curve indicates the location where $D = \Delta_0/2$, which is important in the discussion of T -linear $C_v(T)$ below. $J \equiv J_1 + J_2$.

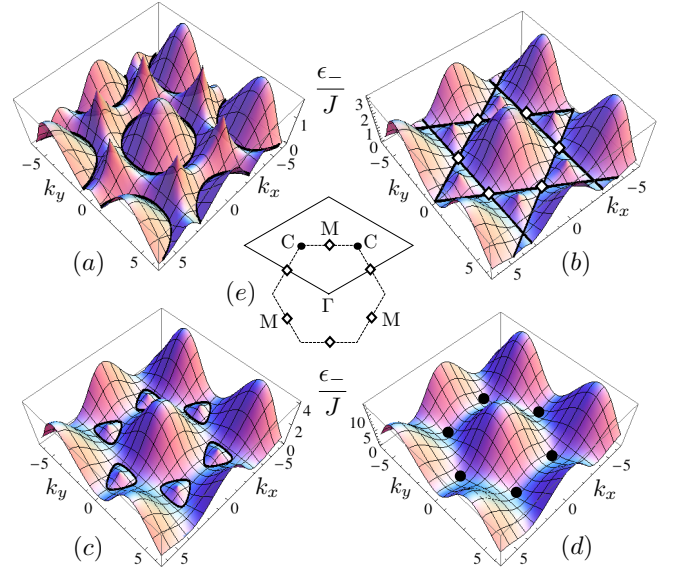


FIG. 3. (Color online) The evolution of the low-energy spin excitations in k_x - k_y plane with $k_z = 0$ at the QCP. The parameters used in the figures are (a) $J_1 = 1.5J_2, D_c = 1.357J$, (b) $J_1 = J_2, D_c = 1.226J$, (c) $J_1 = 0.8J_2, D_c = 1.274J$, (d) $J_1 = 0, D_c = 2.01J$. The low-energy gapless contours are marked with thick black lines in (a-c), while in (d) the low-energy gapless points are marked with black dots. Lattice constants in xy plane are set to 1. (e) is the Brillouin zone (BZ) of the honeycomb lattice. For $J_1 > J_2$, the contour line is centered in the middle of BZ. For $J_1 < J_2$, the contour lines are centered around and eventually shrink to the corners of BZ in the limit $J_1 \rightarrow 0$. The “ \diamond ” points in (b) correspond to “M” points in (e) with $k_z = 0$.

When the left hand side (LHS) of the SPE Eq. (13) is less than 2 for any choice of $\Delta(T)$, the rotor is condensed which signals the presence of magnetic order. Therefore, besides the transition temperature from the high-temperature paramagnetic phase to the low-temperature spin spirals, we also obtain the critical D_c that separates spin spirals from QP phase and the phase diagram at $T = 0$ (see Fig. 2). As expected,

D_c obtained here is smaller than the one determined previously from the Weiss MFT. In particular, D_c/J is minimal at $J_1 = J_2$ corresponding to the largest frustration at this point. Right at the QCP and $T = 0$, $\Delta(0) \equiv \Delta_0 = 3J_2 + J_1^2/J_2$ and the low-energy spin mode $\epsilon_{-,k}$ develops gapless excitations. As shown in Fig. 3(a-d), the momenta of the gapless excitations form contour lines that are identical to the contours of degenerate classical ground state spiral wavevectors in Eq. (4). Moreover, as J_1/J_2 increases from 0, the contour lines around the BZ corners gradually expand and meet at M points when $J_1 = J_2$.

In the vicinity of QCP with $T \ll J$ —At finite T , $\Delta(T)$ increases with temperature and we define $\Delta(T) \equiv \Delta_0 + \Delta_1(T)$. The spin excitation $\epsilon_{\pm}(k)$ also picks up a self-energy via the temperature dependence of $\Delta(T)$. By numerically solving the SPE, we find that, near the QCP $\Delta_1(T) \propto T^2$ at very low temperatures with $T \ll J$. Here, we provide an analytical argument; a similar argument is readily formulated for the quasi-2D limit with $J_1 \ll J_2$. At $T \ll J$, the low-energy spin excitation near the contour lines can be approximated with the dispersion,

$$\epsilon_{-,k} \approx \sqrt{A\Delta_1(T) + v_{\perp,k_0}^2 k_{\perp}^2 + v_{z,k_0}^2 k_z^2} \quad (15)$$

where $A = 4D_c - 2\Delta_0$, k_0 is a momentum coordinate running along the contour lines, k_{\perp} is normal to the tangent of the contour line at k_0 , and we have neglected the weak temperature dependence of the speeds v_{\perp}^2, v_z^2 . Eq. (15) is expected to be a good approximation for $\epsilon_{-}(k)$ less than a cutoff energy Ω with $T \ll \Omega \ll J$. The SPE can be approximated as

$$\int_{k_0, k_{\perp}, k_z}^{\Lambda} \frac{A \coth(\frac{\beta}{2} \sqrt{A\Delta_1(T) + v_{\perp}^2 k_{\perp}^2 + v_z^2 k_z^2})}{2\sqrt{A\Delta_1(T) + v_{\perp}^2 k_{\perp}^2 + v_z^2 k_z^2}} + b = 2, \quad (16)$$

where the integral is over the region around the contour lines with $|k_{\perp}|, |k_z| \lesssim \Lambda$, and b is the approximately T -independent contribution from outside this region. At low temperature, the temperature-dependent part of the integral becomes independent of the cutoff Ω , and only depends on T via the dimensionless parameter $\frac{A\Delta_1(T)}{T^2}$. In order for the integral to be constant in temperature, we thus expect $\Delta_1(T) \propto T^2$ in the limit $T \ll \Omega$. This result immediately leads to the internal energy, which can be approximated as

$$E \sim \int_{k_0, k_{\perp}, k_z}^{\Lambda} \frac{\sqrt{A\Delta_1(T) + v_{\perp}^2 k_{\perp}^2 + v_z^2 k_z^2}}{e^{\beta \sqrt{A\Delta_1(T) + v_{\perp}^2 k_{\perp}^2 + v_z^2 k_z^2}} - 1} \propto T^3 \quad (17)$$

for $T \ll \Omega$. This gives $C_v \propto T^2$ in this temperature regime. This T^2 - C_v regime at low temperatures is confirmed by our numerical results which are shown in Fig. 4(a).

In Fig. 4(a), we also find that, as J_1/J_2 moves to the point $J_1 = J_2$ from either side, the temperature range of the T^2 - C_v regime diminishes. We attribute this to the observation that the $T = 0$ DOS at the QCP increases with energy, then saturates to a roughly constant value. This saturation energy (in units of J) is found to be lowest when $J_1 = J_2$.

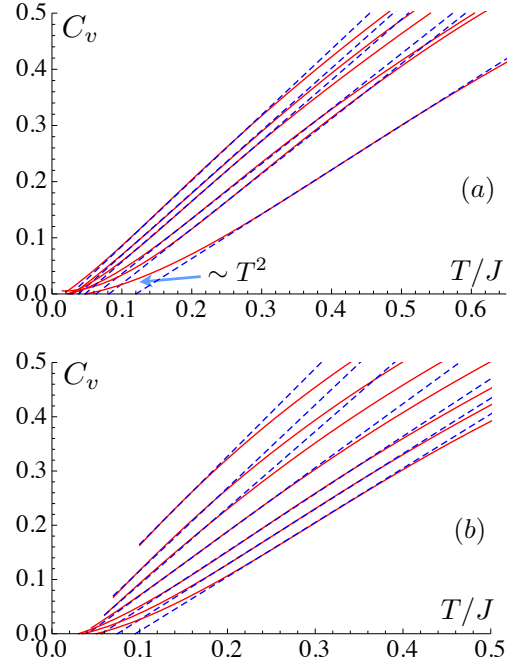


FIG. 4. (Color online) The temperature dependence of C_v in the paramagnetic phase. In (a), from top curve to bottom curve, $J_1 = J_2, 0.7J_2, 1.5J_2, 1.8J_2, 0.3J_2, 0$ with $D \approx D_c$ and $D = 1.24J, 1.311J, 1.36J, 1.472J, 1.576J, 2.01J$, respectively. In (b), $J_1 = 0.5J_2$ and $D = 1.083J, 1.167J, 1.233J, 1.32J, 1.41J, 1.48J, 1.547J$ from top curve to bottom curve. For $J_1 = 0.5J_2$, $D_c = 1.413J$. And $T_c = 0.10J, 0.07J, 0.064J, 0.04J$ for $D = 1.083J, 1.167J, 1.233J, 1.32J$, respectively. The dashed lines are the linear fits for a range of data points. Energy is in units of J .

Linear- T specific heat at intermediate T —In Fig. 4(a) and (b), we find an intermediate temperature regime with $C_v \approx c_1 T + c_0$. To account for this regime, we first note that when $D \approx \frac{\Delta_0}{2}$, the low-energy spin excitation is approximately the square root of a perfect square:

$$\begin{aligned} \epsilon_{-,k} &\approx \sqrt{2|s_{-,k} + D + \frac{\Delta(T)}{2}|} \\ &\approx \sqrt{2(D + \frac{\Delta_1(T) - \Delta_0}{2}) + \frac{k_{\perp}^2}{2m_{\perp,k_0}} + \frac{k_z^2}{2m_{z,k_0}}} \end{aligned} \quad (18)$$

If $D = \frac{\Delta_0}{2}$, such dispersion on contour lines in 3D gives a constant DOS at low energies and, because $\Delta(T)$ is only weakly T -dependent in this case, this leads to $C_v \propto T$ at low temperatures. This conclusion also holds in the 2D limit $J_1 \ll J_2$. As shown in Fig. 2, D_c is slightly greater than $\frac{\Delta_0}{2}$ and the system at $D = \frac{\Delta_0}{2}$ is magnetically ordered at very low temperatures. Once the system enters into the paramagnetic phase, a linear- T C_v is obtained, which is shown as the top curve in Fig. 4(b). Moreover, this linear- T C_v regime persists even when D is increased to or slightly beyond D_c .

Discussion—Here we discuss the experiments of Ref. 15 in terms of our proposal that the system is proximate to a QCP. The spin susceptibility is observed to saturate to a constant below 25K, which is consistent with our theoretical predic-

tion in Eq. (9). Experiments also find a power-law specific heat $C_v(T) \simeq \gamma T^\eta$ with $\eta \approx 1.0(1)$ for $0.35\text{K} < T < 7\text{K}$ (or $0.02J < T < 0.34J$)[15]. Determination of both these behaviors relies on the subtraction of a magnetic impurity contribution, which may be delicate, and which has significant effect below about 25 K and 1 K for the susceptibility and specific heat, respectively. As shown in Fig. 4, the range of the linear- T specific heat observed in experiments is compatible with our results with $J_1 \sim J_2$. Taking $J_1 = J_2$ and $D = D_c$, we find the powder-averaged zero temperature spin susceptibility $\chi_0^{\text{av}} \approx 0.0125\text{emu/mol}$, which is very close to the experimental value 0.013emu/mol . Moreover, the coefficient γ in $C_v(T)$ is found to be 208mJ/mol-K^2 at $J_1 = J_2$ while the experimental value is 168mJ/mol-K^2 . Our calculation gives a Wilson ratio of 4.36, not far from the experimental value 5.6[15]. The agreement can be further improved by slightly adjusting J_1/J_2 and D .

6H-B may lie either on the QP or magnetically ordered side of the QCP. At very low temperatures we thus expect either a small energy gap, or the onset of spiral magnetic order. It should be noted that the presence of magnetic impurities may interfere with observation of such very-low-temperature behavior. To detect the energy gap or magnetic order, NMR or μSR measurements may be helpful. If the system is in the QP phase, then in a single crystal sample we predict $\chi^z = 0$ and $\chi^\perp = \text{const}$ at zero temperature. In Ref. 16, the authors considered a state with gapped $S^z = \pm 1$ fermions and gapless $S^z = 0$ fermions forming a gapless Fermi surface. This state has a spin gap, with thermodynamic properties dominated by the gapless Fermi surface. The two QSLs proposed by Ref. 17 have gapless spin excitations. These states are thus distinct from the QP phase of our proposal, which has a fully gapped spectrum. Especially if single crystal samples become available, inelastic neutron scattering should be able to further distinguish these proposals by measuring the dispersion

of low-energy spin excitations; our prediction is depicted in Fig. 3.

To summarize, in this work we propose a minimal J_1 - J_2 - D model for 6H-B- $\text{Ba}_3\text{NiSb}_2\text{O}_9$ and argue that the “QSL” phenomena in the system is due to the proximity to a quantum critical point. Despite the simplicity of the model, our theoretical prediction is broadly compatible with current experiments[15]. A number of future directions for experiments are suggested.

Acknowledgements—G. C. thanks L. Balicas for useful discussion. This research is supported by the David and Lucile Packard Foundation (G.C. and M.H.) and by the NSF through grant no. DMR-1001240 (G.C. and L.R.).

-
- [1] L. Balents, *Nature* **464**, 199 (2010).
 - [2] J. Gardner *et al*, *Phys. Rev. Lett.* **82**, 1012 (1999).
 - [3] Z. Hiroi *et al*, *J. Phys. Soc. Jpn.* **70**, 3377 (2001).
 - [4] Y. Shimizu *et al*, *Phys. Rev. Lett.* **91**, 107001 (2003).
 - [5] J. S. Helton *et al*, *Phys. Rev. Lett.* **98**, 107204 (2007).
 - [6] Y. Okamoto *et al*, *Phys. Rev. Lett.* **99**, 137207 (2007).
 - [7] T. Itou *et al*, *Phys. Rev. B* **77**, 104413 (2008).
 - [8] Y. Okamoto *et al*, *J. Phys. Soc. Jpn.* **78**, 033701 (2009).
 - [9] M. de Vries *et al*, *Phys. Rev. Lett.* **104**, 177202 (2010).
 - [10] M. Kohno *et al*, *Nature Physics* **3**, 790 (2007).
 - [11] O. A. Starykh *et al*, *Phys. Rev. B* **82**, 014421 (2010).
 - [12] E. Stoudenmire *et al*, *Phys. Rev. B* **79**, 214436 (2009).
 - [13] G. Chen *et al*, *Phys. Rev. Lett.* **102**, 096406 (2009), G. Chen *et al*, *Phys. Rev. B* **80**, 224409 (2009).
 - [14] R. R. P. Singh, *Phys. Rev. Lett.* **104**, 177203 (2010).
 - [15] J. Cheng *et al*, *Phys. Rev. Lett.* **107**, 19720 (2011).
 - [16] M. Serbyn *et al*, arXiv:1108.3070 (Unpublished).
 - [17] C. Xu *et al*, arXiv:1110.3328 (Unpublished).
 - [18] A. Mulder *et al*, *Phys. Rev. B* **81**, 214419 (2010).
 - [19] J. M. Luttinger and L. Tisza, *Phys. Rev.* **70**, 954964 (1946).